Zachary F. Johnson (zachary.f.johnson@cmich.edu)
Department of Earth and Atmospheric Sciences, Central Michigan University, Mt. Pleasant, Michigan, USA,
Department of Earth, Atmospheric, and Space Sciences, Purdue University, West Lafayette, Indiana, USA

Daniel R. Chavas
Department of Earth, Atmospheric, and Space Sciences, Purdue University, West Lafayette, Indiana, USA

Jhordanne J. Jones
Department of Earth, Atmospheric, and Space Sciences, Purdue University, West Lafayette, Indiana, USA

Yoshimitsu Chikamoto
Department of Plants, Soils, and Climate, Utah State University, Logan, Utah, USA

Hamish A. Ramsay
CSIRO Environment, Aspendale, Victoria, Australia

This paper is a non-peer reviewed preprint submitted to EarthArXiv.

Impacts of zonal SST gradients on subtropical highs and implications for early season tropical cyclone landfall frequency

Zachary F Johnson,[a,b] Daniel R. Chavas,[b] Jhordanne J. Jones,[b] Yoshimitsu Chikamoto,[c] Hamish A. Ramsay,[d]

[a] *Department of Earth and Atmospheric Sciences, Central Michigan University, Mt. Pleasant, Michigan, USA*

[b] *Department of Earth, Atmospheric, and Space Sciences, Purdue University, West Lafayette, Indiana, USA*

[c] *Department of Plants, Soils, and Climate, Utah State University, Logan, Utah, USA*

[d] *CSIRO Environment, Aspendale, Victoria, Australia*

Corresponding author: Zachary F. Johnson, zachary.f.johnson@cmich.edu

ABSTRACT: Tropical cyclone (TC) seasonal landfall probability is challenging to forecast because of the limited seasonal predictability of steering flow patterns. Past studies mainly focus on the large-scale ocean and atmospheric conditions that lead to changes in seasonal tropical cyclone genesis frequency in a given basin, but less attention has focused on seasonal landfall probability inherent to changes in steering flow patterns linked to subtropical highs (STHs). Here, we examine SST anomaly patterns that control variability in summertime STH cells in the northern and southern hemispheres. We link those ocean impacts to changes in early-season TC landfall probability in the Western North Pacific, North Atlantic, and South Indian Ocean basins. STHs in the North Pacific, North Atlantic, and South Indian Ocean exhibit increased variability on their western peripheries linked to anomalous zonal SST gradients. In the northern hemisphere, an inter-basin zonal contrast in SST anomalies fosters a westward extension in both North Pacific and North Atlantic STHs. As a result, TCs curve around STHs $\sim 6°$ in longitude farther west in the Western North Pacific basin. In contrast, the Atlantic basin had the opposite effect due to minimal TC activity over the tropical Atlantic from inhibiting SST anomalies. The South Indian Ocean had a 9% increase in landfall probability for TCs that formed in the western half of the Southern Indian Ocean during a positive localized SST dipole. The seasonal persistence of southern hemispheric STHs resembles aquaplanet simulations of STHs, in contrast to the seasonal evolution observed in their northern hemispheric counterparts.

1. Introduction

During northern and southern hemispheric summers, atmospheric subtropical high (STH) cells have a significant effect on weather and climate patterns (Shuqing and Ming 1999; Wu et al. 2005; Gamble et al. 2008; Choi et al. 2016; Gilliland and Keim 2018). These subtropical highs are regions of semi-permanent high-pressure systems, typically between 20 and 40° in latitude in each hemisphere (Seager et al. 2003; Miyasaka and Nakamura 2010). They are primary contributors to poleward heat transport through atmospheric and oceanic circulations (Seager et al. 2003; Miyasaka and Nakamura 2010; Yun et al. 2015; Huang et al. 2015). They also influence the likelihood and location of tropical cyclone landfall due to their effect on steering flow (Camp et al. 2019). As such, variability in STHs induces changes in seasonal tropical cyclone landfall probability (Johnson et al. 2022).

In the northern hemisphere (NH), STH systems are located in the North Pacific and North Atlantic, while in the southern hemisphere (SH), STHs are located in the South Indian Ocean, South Pacific, and South Atlantic (Seager et al. 2003). On the equator side of STHs, easterly wind stress promotes warm water to pile up on the western part of basins, contributing to basin-wide zonal SST gradients in the tropics: warm waters in the western side of the basins and cool waters in the eastern side. As a result of this zonal SST gradient, warm waters toward the west lead to surface atmospheric destabilization, low surface pressure, and ascending motion, while the cool waters to the east lead to a stable atmosphere, high pressure, and descending motions. To satisfy the Sverdrup balance, STHs accompany poleward wind on the western side under ascending motion and equatorward wind on the eastern side under descending motion (Sverdrup et al. 1942; Rodwell and Hoskins 2001; Seager et al. 2003), expressed in Equation 1:

$$\beta v \approx f \frac{\partial \omega}{\partial p} \tag{1}$$

where v is the meridional wind, ω is the vertical velocity, f is the Coriolis parameter, and β is the meridional gradient of f. Hence, the anticyclonic circulation of the subtropical high and the zonal SST gradient (warm west / cold east) constitute a stable atmosphere-ocean system in which each feature helps to sustain the other. Any perturbation in this system, particularly changes in the zonal SST pattern, may lead to STH changes and therefore changes in TC tracks and landfall probability.

Given that zonal SST gradients contribute to the STH, it is reasonable to expect anomalous zonal SST gradients constrained to the western edge of a basin may drive a westward extension of the STH. Past work has indeed shown that SST anomalies can force shifts in the STH (e.g., Lu and Dong 2001; Wu et al. 2010; Wang et al. 2013; Kosaka et al. 2013; He and Zhou 2015; Wright et al. 2022; Jones et al. 2024).

Climatological STHs depict flow curving from westward to poleward around the western periphery of the STH, commonly where we have warm waters and abundant TC activity. However, the western edge of STHs exhibit significant variability in both the wind and 850 hPa geopotential (Z850) height field. For instance, Wang et al. (2013) describe a region in the western North Pacific (15°N–25°N, 115°E–150°E) with the highest variance in Z850 anomalies, which they use to define a Western North Pacific High (WPSH) index. They found a significant relationship between the WPSH and the number of TCs making landfall in Southeast Asia. They attribute WPSH variability to a zonal inter-basin SST dipole in the north tropics band (10–20°N), linking the north Indian Ocean and western North Pacific, also supported by subsequent studies (Li et al. 2020). Such analyses have not been applied to STHs in other ocean basins. Therefore, a question remains whether similar SST anomaly patterns explain variability on the western edges of STHs in other basins and if they have an impact on TC landfall probability. There is value in comparing results across basins, particularly between both hemispheres, given that the midlatitude flow is much more zonally variable in the northern hemisphere as compared to the southern hemisphere owing to the contrasting distribution of land and topography (Broccoli and Manabe 1992; Wang and Ting 1999; Shaw et al. 2022).

Here, we quantify the magnitude of variability on the western part of STHs in the North Pacific, North Atlantic, South Indian Ocean, South Pacific, and South Atlantic. We then quantify the relationship to SST anomaly patterns and TC landfall probability in the North Pacific, North Atlantic, and South Indian Ocean. We will address the following questions:

1. What SST anomaly patterns control variability on the western peripheries of STH cells in the northern and southern hemispheres?

2. How does TC landfall probability vary with respect to SST patterns relevant to STHs in the North Pacific, North Atlantic, and South Indian Ocean basins?

3. What are the key differences and similarities between northern and southern hemispheric STHs?

To answer these questions, we first apply an empirical orthogonal function (EOF) analysis to the Z600 anomaly field in each basin from June-August in the northern hemisphere and December-February in the southern hemisphere to quantify STH variability and then explore their dependencies on SST patterns. Next, we composite seasons when STHs extend to the west or are retracted to the east based on such SST patterns. We identify three basins with abundant TC activity and significant variability on the western edge of the basin's STH: The North Pacific, North Atlantic, and South Indian Ocean. We use the composite seasons to examine TC activity and whether there is an effect on seasonal landfall probability in the aforementioned basins. We explain the EOF analysis and our data in Section 2. Then we describe our results of the EOF analysis and changes in TC landfall in 3, followed by a discussion with concluding remarks in Section 4.

2. Data and methods

a. Reanalysis data

To assess the height field associated with STHs, we obtain European Centre for Medium-range Weather Forecasts (ECMWF) reanalysis ERA5 monthly 850 and 600 hPa geopotential height (Z850 and Z600), horizontal winds at 850 and 600 hPa (UV850 and UV600), and 500 hPa vertical velocity ($\omega 500$) and calculate anomalies based on the 1978–2020 mean (Hersbach 2016). $\omega 500$ anomalies are used as a proxy for tropical deep convection and vertical velocity gradients $\frac{\partial \omega}{\partial p}$, similar to past studies (e.g., Maloney and Esbensen 2003; Liess and Geller 2012; Li et al. 2023). These ERA5 datasets have $0.25° \times 0.25°$ resolution. Additionally, we use the Centennial in-situ Observation-Based Estimate SST (COBE-SST; $1° \times 1°$ resolution) (Ishii et al. 2005) to calculate anomalies based on the 1978–2020 mean. We limit ERA5 and COBE-SST datasets to the June-August season (JJA) in the northern hemisphere and December-February (DJF) in the southern hemisphere for the following analyses. The linear trends at each grid point are extracted from the anomalies to remove the long-term trend, such as the global warming component.

b. Tropical cyclone data

TC data are obtained from the International Best Tracks Archive for Climate Stewardship version 4 (IBTrACSv4) (Knapp et al. 2010). Western North Pacific (WNP) and North Atlantic (NA) basin TCs are extracted in the IBTrACSv4 dataset from 1979–2020 during the May–September (MJJAS) season. Southern Indian Ocean (SIO) basin TCs are extracted in the IBTrACSv4 dataset from 1978–2020 during the November–March (NDJFM) season. We define landfall based on whether the TC passes over or within 25 km of specified coastlines: Philippines, Vietnam, Cambodia, Laos, China, Taiwan, South Korea, North Korea, Japan, and Russia for the WNP, United States, Canada, Mexico, Belize, Guatemala, Honduras, El Salvador, Nicaragua, and Costa Rica for NA, and Madagascar and Mozambique for SIO basins. Because of the sparse 6-hourly data from IBTrACSv4, we interpolate enough points between each observation in IBTrACSv4 to test if tracks intersect or pass over a coastline through a spline function. Next, we define $N_{genesis}$, $N_{landfall}$, and $p_{landfall}$ for the number of TCs, landfalls, and the probability of landfall (i.e., landfall fraction) to test the effect of climate patterns on these variables. If a TC makes multiple landfalls, it still only counts as one landfall. This study only counts TCs that achieve tropical storm status (> 17.5 ms^{-1}). Long-term trends of TC genesis and landfall are not removed for the following analysis.

This study composites TC tracks; therefore, we define mean composite track. Each track is interpolated into 400 equally-spaced points, so the distance between each point is dependent on the individual TC track. For instance, a 1600 km track would have a 4 km distance between each point, whereas a 400 km track will have a 1 km distance between each point. Next, this study averages across each of the 400 points to produce a mean composite track. Hence, the mean track estimates the mean trajectory for composite seasons and also provides the mean genesis and dissipation locations.

c. EOF analysis of Z600 anomaly field

To quantify the changes in location, structure, and strength of STHs, we statistically decompose the detrended seasonal Z600 anomaly field by applying an empirical orthogonal function (EOF) analysis. We chose the 600 hPa level to capture the deeper tropospheric winds (DeMaria et al. 2022). In the Western North Pacific basin, we apply the EOF analysis on the western edge of the North Pacific STH in the same region as Wang et al. (2013) (10°–30°N,100°–180°E). Past work has primarily focused on the North Pacific STH. Here, we extend a similar analysis to other basins for a direct intercomparison of the STH. We apply the EOF analysis over the central and western North Atlantic (10°–40°N,90°–30°W). We apply the EOF analysis over the whole basin in the South Indian Ocean (10°–35°S,35°–115°E) and the South Pacific (10°–30°S,150°E–90°W). Lastly, over the South Atlantic, we apply the EOF analysis over the entire subtropics (10°–30°S,50°W–10°E).

3. Results

a. Seasonal evolution of the STH

The monthly evolution of STH cells is shown in Figure 1. In the northern hemisphere (NH), the boreal winter Z850 height field depicts pure zonal flow with very weak meridional pressure gradients equatorward of the jet stream (Fig. 1a,b). A zonal band of increased heights comprised of small, weak closed high-pressure centers confined to the eastern portion of the basins emerges in boreal winter in the northeastern Pacific and north-central Atlantic. Through boreal spring, these high-pressure centers expand westward across their respective basins and strengthen (Fig. 1c-e). By boreal summer, the STH cells are elongated in an SW-NE structure and reach peak strength (Fig. 1f-h). On the western periphery of these STH cells exist regions of increased Z850 variability during boreal summer months, particularly in the western North Pacific, where a lobe of increased variability extends from the mid-latitudes toward the subtropical western North Pacific (Fig. 1f-i). By boreal fall, the STH weakens, becoming zonally symmetric (Fig. 1i-k).

Southern hemispheric seasonal evolution of STHs exhibit differences compared to northern hemisphere STHs. First, the seasonal evolution of the South Pacific STH is much more stable in structure and location throughout the year, only increasing in strength during the Austral summer (Fig. 1i,a,b). However, the South Atlantic and South Indian Ocean STH cells have significant seasonal evolution in location, structure, and strength. Both the South Atlantic and South Indian Ocean STH centers emerge off South America and Africa in austral spring (Fig. 1h-k), respectively. They shift eastward toward the center of their respective basins during austral summer, depicted by zonally symmetric ellipsoid structures (Fig. 1a,b,l). Note that this zonal evolution is in contrast to the NH cells that start on the eastern edge of the basin and expand westward toward summer. They retreat back west over South America and Africa in austral fall (Fig. 1b-e). Similar to the northern hemispheric STH cells, the South Indian Ocean, South Atlantic, and South Pacific

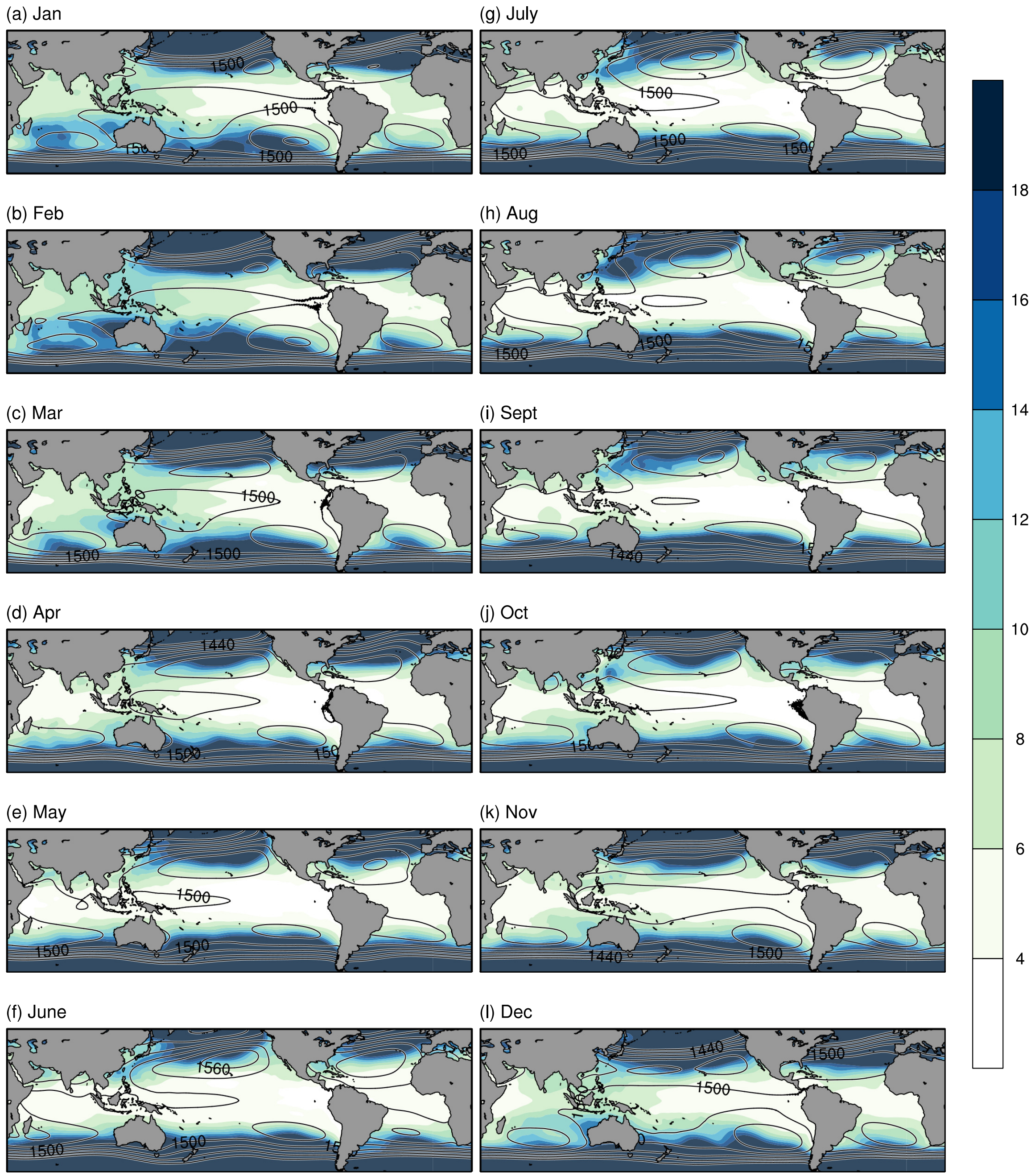

FIG. 1. Monthly climatological Z850 (contours) based on a 1978–2020 mean and monthly standard deviations (colors). Contour stride is every 30 m.

STHs show lobes of increased variability extending equatorward on their western peripheries during the austral summer (Fig. 1l,a,b,c). Specifically, the South Indian Ocean is characterized by increased variability near Madagascar in December-March (Fig. 1l,a,b,c). The South Pacific

STH has increased variability over the central and western South Pacific (Fig. 1l,a,b). In the South Atlantic, an equatorward increase in variability occurs east of South America (Fig. 1k,l,a,b,c). These results point to the Z850 field exhibiting more variability on the western peripheries of STH cells in both hemispheres. This Z850 variability on the western edges of STHs can be characterized as a westward extension or retraction on its western periphery. We next examine the dependencies of this variability to SST anomaly patterns.

b. Variability in the western peripheries of northern hemispheric STH cells

Based on the potential impact of STH cells on TC landfall probability noted in previous studies (e.g., Wang et al. 2013; Camp et al. 2019; Johnson et al. 2022), combined with the variability noted on the western edges of STH cells in Figure 1, we analyze modes of variability of STH cells in the North Pacific, North Atlantic, South Pacific, South Atlantic, and South Indian Oceans via EOF analysis of the Z600 height anomaly field during boreal and austral summers. The 600 hPa level is chosen because DeMaria et al. (2022) points out that the steering of tropical cyclones is not dominated by lower tropospheric flow where STHs are typically defined, but rather deep tropospheric flow at ~550–600 hPa. To account for ocean-atmosphere coupling at the lower level but also incorporate the deeper troposphere steering flow, we apply the following analysis at 600 hPa.

In the northern hemisphere, the first modes of the western periphery of STH variability account for ~ 43 and $\sim 48\%$ of explained variance for the North Pacific and North Atlantic (Fig. 2a,e). In the WNP, the positive phase is characterized by an anomalous anticyclonic circulation superimposed on the western edge of the STH, extending from the central North Pacific to Southeast Asia, similar to the findings of Wang et al. (2013). The first mode of the NA depicts a strengthened STH combined with positive Z600 anomalies extending over North America (Fig. 2e). Both leading modes of STH variability are commonly referred to as the westward extension of the STH (e.g., Lu and Dong 2001; Zhou et al. 2009). The first modes of the North Pacific and North Atlantic STH accompany a zonal inter-basin SST anomaly dipole in the north tropical region: negative anomalies south of the STH and positive anomalies in the basin adjacent to the west (Fig. 2b,f). For instance, the westward extension of positive height anomalies for the North Pacific STH covaries with positive SST anomalies extending from the North Indian Ocean to the South China

Sea and negative SST anomalies between 150°E and Hawaii. Similarly, the westward extension of positive height anomalies from the Atlantic STH covaries with positive SST anomalies between Hawaii and mainland Mexico and negative in the north tropical Atlantic (Ham et al. 2013; Stuecker 2018).

Based on the inter-basin zonal contrast in SST revealed when regressing both PC1s onto SST anomalies, we compute an Indo-Pacific dipole index by finding the difference between the North Indian Ocean to South China Sea SST anomalies (5°N–20°N, 50°E–120°E) and WNP anomalies (5°N–20°N, 150°E–180°): a similar index is previously developed by Wang et al. (2013) in Figure 3a. Likewise, we compute a similar index based on the NA PC1 regressed on SST anomalies in the North Atlantic and northeastern Pacific by computing the difference in SST anomalies in the northeast tropical Pacific (10°N–25°N, 150°W–120°W) and the North Tropical Atlantic (NTA) region (10°N–25°N, 70°W–20°W) in Figure 3b. As a result, both of these indices define northern tropical inter-basin SST contrasts with the positive phase characterized by positive SST anomalies to the west and negative ones to the east. These inter-basin anomalous SST dipoles correlate with their respective principal components from the EOF analysis: $R = 0.78$ for the WNP (Fig. 3a) and $R = 0.51$ for the NA (Fig. 3b).

In Figure 4, we present composite years based on positive and negative SST gradient indices using Z850 full field to analyze STH spatial extent variations, as 850 hPa is the most common level in past work to represent the STH. Similar to Figure 2, a positive zonal inter-basin SST dipole is characterized by a westward extension of the STH cells in the North Pacific and North Atlantic basins. In the Western North Pacific, the 850 hPa 1515 geopotential meter contour extends $\sim 15°$ in longitude farther west during the positive composites versus the negative composites. In the North Atlantic, the 850 hPa 1560 geopotential meter contour extends $\sim 12°$ in longitude farther west during positive composites versus negative composites. The westward extension of the STH is not simply a westward shift of the STH circulation but rather an anomalous anticyclonic circulation superimposed on the western edge of the STH.

Based on westward extensions of the North Atlantic and North Pacific STHs during an inter-basin zonal SST dipole in the 10°–20°N band, Figure 4 shows a change in the flow pattern on the western edges of the STH cells. In the WNP, Figure 4e and Figure 2a depict anomalous easterlies between the equator and $\sim 20°$N. These easterlies extend over the North Indian Ocean, where positive

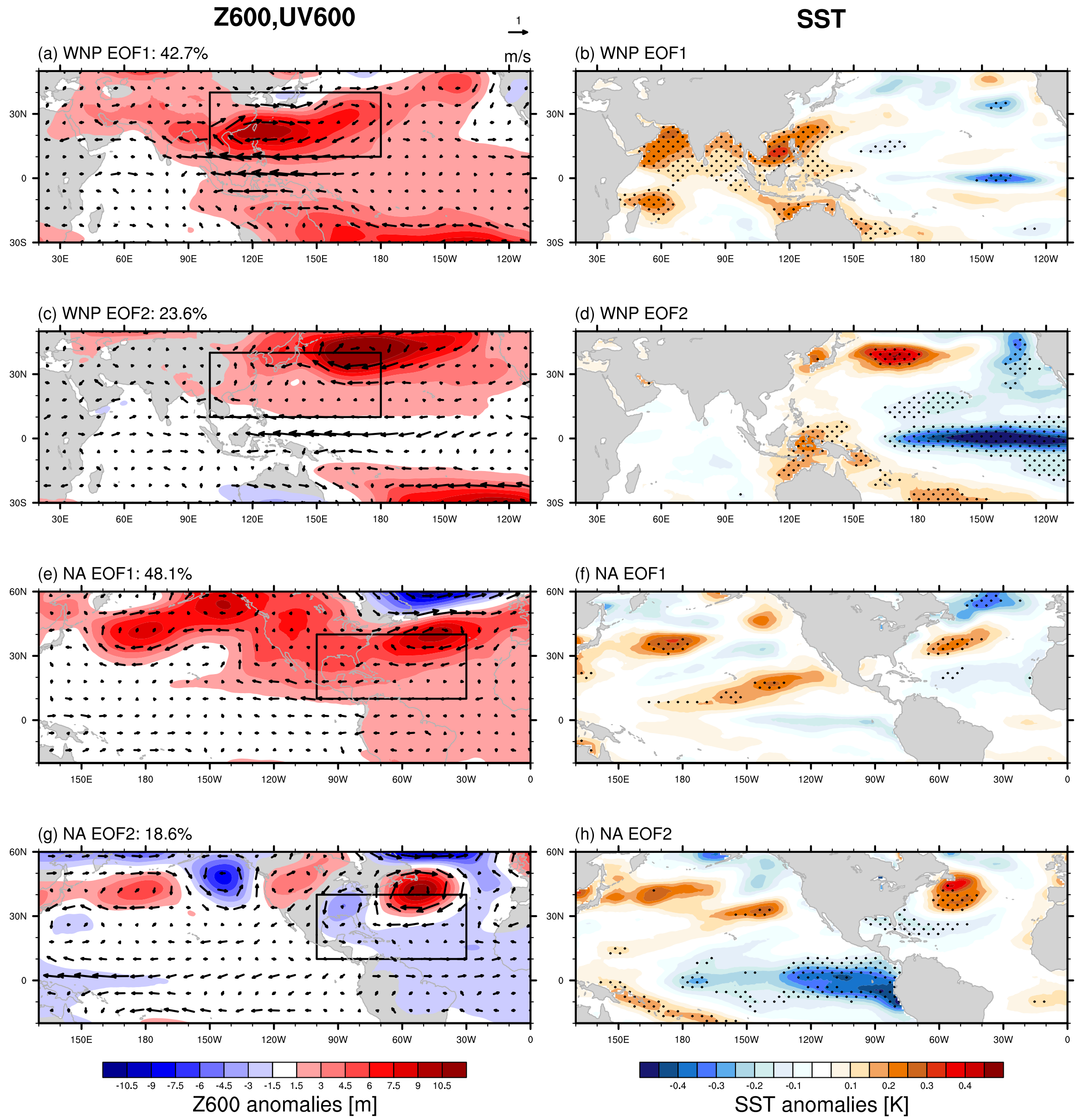

FIG. 2. The first and second modes of the Z600 anomaly field (box region) in the (a,c) Indo-Pacific sector and the (e,g) west-central North Atlantic during June–August via EOF analysis. Respective PC1 and PC2 regressed on the Z600 and UV600 anomaly fields for the (a,c) Indo-Pacific (e,g) and North Atlantic-eastern North Pacific. Similarly, PC1 and PC2 regressed on SST in the (b,d) Indo-Pacific and (f,h) North Atlantic-Eastern North Pacific sector. The dotted region indicates statistical significance above the 95% level using Student's t-test for SST anomalies.

Z850 and SST anomalies exist. Meanwhile, in the North Atlantic, Figure 4f and Figure 2e show anomalous easterlies in the ~ 5°–25°N region extending from ~ 30°W-120°W. In other words,

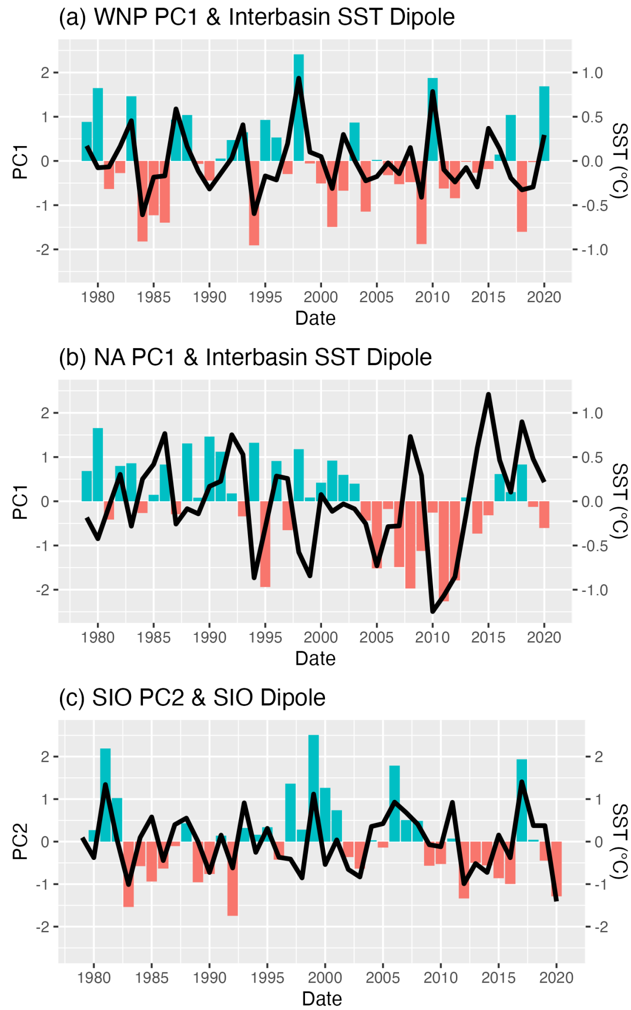

FIG. 3. (a) PC1 extracted from Fig. 2a (bars: left-axis) and Indo-Pacific SST Dipole time series (line: right-axis), (b) PC1 extracted from Fig. 2e (bars: left-axis) and Pacific-Atlantic dipole time series (line: right-axis), and (c) PC2 extracted from Fig. 6c (bars: left-axis) and SST dipole in the Southern Indian Ocean (line: right-axis). The (a) Indo-Pacific dipole is defined as the difference between North Indian Ocean (5°N–20°N, 50°E–120°E) and WNP (5°N–20°N, 150°E–180°) SST anomalies. The (b) Pacific-Atlantic dipole is defined as the difference between the northeast tropical Pacific (10°N–25°N, 150°W–120°W) and the North Tropical Atlantic (NTA) region (10°N–25°N, 70°W–20°W) SST anomalies. The (c) SIOD is defined as the difference between southwest South Indian Ocean (25°N–35°S, 50°W–80°E) and the northeast South Indian Ocean (10°N–20°S, 60°W–90°E) SST anomalies.

during a positive zonal SST dipole, anomalously warm west and cold east, we see anomalous easterlies over the central NTA region, extending through the Caribbean and Central America to

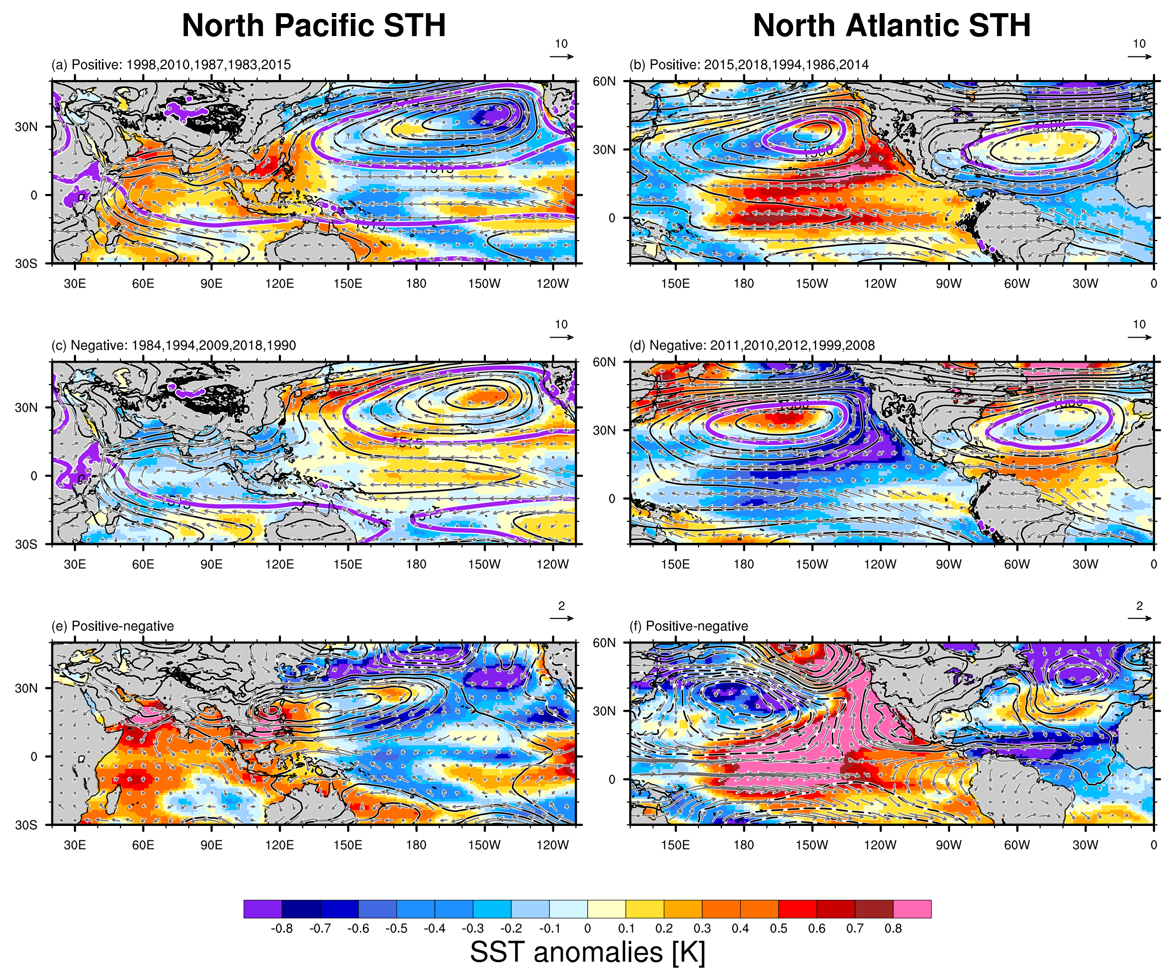

FIG. 4. (a,c) Indo-Pacific SST dipole and (b,d) Pacific-Atlantic dipole composite seasons using SST anomalies (colors), Z850 (contours), and UV850 (arrows). Contours are every 15 geopotential meters. The 1515 m contour is in purple to depict the North Pacific STH and the 1560 m contour for the North Atlantic STH. Arrows are in m/s and defined at the top right of each plot. (e,f) The relative difference between positive and composite seasons consists of contours every 4 geopotential meters.

the northeastern tropical Pacific. The physical justification for anomalous cross-basin easterlies stems from an anomalous zonal inter-basin SST gradient (cold east and warm west) forcing an anomalous zonal pressure gradient (high east and low west) on the southwestern periphery of the STH (Chikamoto et al. 2015; Cai et al. 2019). At the ocean-atmosphere interface, stronger easterly winds over the tropical Atlantic may contribute to amplifying or reinforcing cooling through ocean mixing and turbulence through a positive feedback mechanism. Whereas, in the Western

North Pacific, stronger easterly winds over the monsoon region may cause less ocean mixing and turbulence due to weaker surface winds (Knaff 1997; Wang and Lee 2009).

A possible secondary mechanism to physically explain the westward extensions of the North Atlantic and North Pacific STH is through Sverdrup effects responding to anomalous inter-basin SST gradients (Sverdrup et al. 1942). On the eastern side of the anomalous anticyclonic circulation, accompanying the anomalous negative SSTs in the western North tropical Pacific (170°E, 20°N), Figure 4e depicts anomalous 850 hPa equatorward flow underlying anomalous descending motion at 500 hPa (Fig. 5e). Since this descending motion corresponds to the negative value of $\frac{\partial \omega}{\partial p}$ in the lower troposphere, this feature satisfies the anomalous Sverdrup framework. On the western side of the anomalous anticyclonic circulation (110°E, 20°N), Sverdrup effects are not applicable because no positive value of $\frac{\partial \omega}{\partial p}$ in Figure 5e, possibly obscured by East Asia land effects. Accompanying the negative SST anomalies in the North Atlantic (65°W, 20°N), Figure 4f also depicts anomalous 850 hPa equatorward flow underlying anomalous descending motion at 500 hPa. This descending motion corresponds to the negative value of $\frac{\partial \omega}{\partial p}$ in the lower troposphere, also supporting the anomalous Sverdrup framework like in the western North Pacific. Accompanying the positive SST anomalies in the eastern North Pacific (130°W, 15°N), Figure 4f depicts anomalous 850 hPa poleward flow underlying anomalous ascending motion at 500 hPa. Since this ascending motion corresponds to the positive value of $\frac{\partial \omega}{\partial p}$ in the lower troposphere, this feature also satisfies the anomalous Sverdrup framework. The combined effects of the anomalous easterlies equatorward of STHs in the northern hemisphere responding to off-equatorial interbasin SST and pressure gradients and the anomalous meridional motions reveal an anomalous anticyclonic circulation superimposed onto the western side of northern hemispheric STHs. As a result, the STH ”appears” to extend west when characterizing the STH as isohypses in Figure 4a-b.

Alternatively, the anomalous anticyclonic circulation in the WNP is associated with decaying El Niño summers, linked to Kelvin wave propagation from an anomalously warm Indian Ocean (Zhan et al. 2011; Du et al. 2011; Chung and Li 2015). Analyzing lag regression maps of PC1 in Figure 3a supports this physical mechanism (not shown). Meanwhile, the second modes of June-August Z600 anomalies account for $\sim$ 24 and $\sim$ 19% of explained variance in both the western North Pacific and North Atlantic, respectively. They depict a La Niña effect characterized by a meridional Z600 dipole in both the North Pacific and North Atlantic. They reflect a shifting of the STH center

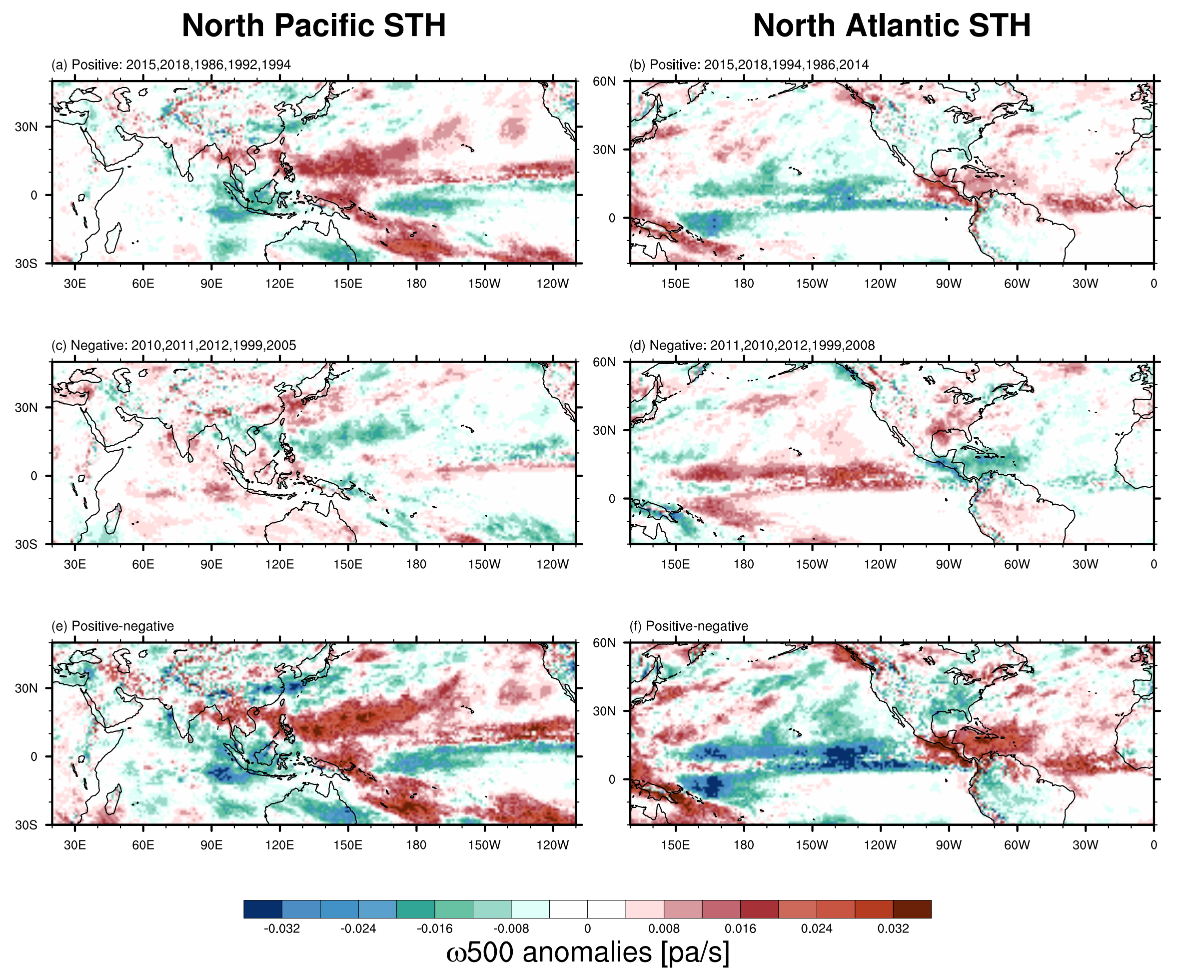

Fig. 5. (a,c) Indo-Pacific SST dipole and (b,d) Pacific-Atlantic dipole composite seasons using ω500 anomalies. (e,f) The relative difference between positive and composite seasons

rather than its westward extension. Since our focus is on TC landfall associated with the westward extensions of STHs, we will disregard these second modes in this context.

c. Variability in the western peripheries of southern hemispheric STH cells

In contrast to northern hemisphere STHs that show westward extensions in their leading modes, the first modes of southern hemispheric subtropical high variability depict monopole patterns, signifying the weakening or strengthening of the STH cells in the southern hemisphere (Figs. 6 and 1). The UV600 anomaly field captures changes in the strength of these STHs. These first modes account for ~69%, 44%, and 44% of explained Z600 variance for the South Indian Ocean, South Pacific, and South Atlantic STHs, respectively (Fig. 6a,e,i). The second modes show more diverse patterns (Fig. 6c,g,k). In the South Indian Ocean, the EOF2 pattern depicts a zonal dipole in the Z600 anomaly field accounting for ~ 16% of STH variability (Fig. 6c). This pattern can be described as a zonal shift of the South Indian Ocean STH. EOF2 in the South Pacific also shows a zonal dipole in the Z600 anomaly field (Fig. 6g). EOF2 in the South Atlantic depicts a meridional structure characterized by a cyclonic anomaly in the midlatitudes and positive Z600 anomalies in the tropics (Fig. 6k).

EOF1 for the South Indian Ocean, EOF2 for the South Pacific, and EOF1 for the South Atlantic strongly correlate with the Niño 3.4 index ($R = 0.76$, 0.71, and 0.61, respectively). Additionally, these modes are highly related to each other ($R > 0.6$). In other words, an El Niño is characterized by a large region of subsidence over the Indo-Pacific region due to its effect on the global Walker circulation, as shown in EOF1 and EOF2 in the Southern Indian Ocean and South Pacific, respectively (Fig. 6a and g). Additionally, these modes of STH variability are consistent with a Matsuno-Gill-like circulation (Matsuno 1966; Gill 1980), characterized by off-equatorial Rossby waves and Kelvin waves responding to El Niño-like warming (Ho et al. 2006).

In addition to the ENSO effect in EOF1, EOF2 in the South Indian Ocean covaries with an SST dipole in that basin, termed the Subtropical Indian Ocean SST Dipole or Southern Indian Ocean Dipole (SIOD) (Behera et al. 2000; Behera and Yamagata 2001; Reason 2001; England et al. 2006; Ho et al. 2006). Its positive phase is characterized by positive SST anomalies south and east of Madagascar and negative SST anomalies west of Australia, reflecting the southwest-northeast SST dipole shown in Figure 6d (note the SIO EOF2 shows a negative SIOD-like pattern). Based on the westward extension of STHs in the northern hemisphere linked to inter-basin SST dipoles, we examine the relationship with the South Indian Ocean STH more closely in Figure 7 by compositing the five strongest positive and five strongest negative phases of dipole strength (Fig. 6). In its positive phase in Figure 7a, the South Indian Ocean STH is stronger and expanded toward the northwest (i.e., the 1530 m contour is ~ 3° in longitude farther west compared to the negative composite in Fig. 7c). A stronger meridional pressure gradient exists on the northern edge of the STH accompanying stronger easterly winds in the 5 – 25°S band from the central Southern Indian Ocean toward Madagascar and Mozambique (Fig. 7e). The difference between positive and negative composites (Fig. 7e) clearly shows this zonal shift in the Z850 height field, related both to a zonal shift in the STH and a strengthening of the STH center. The composite difference depicts a

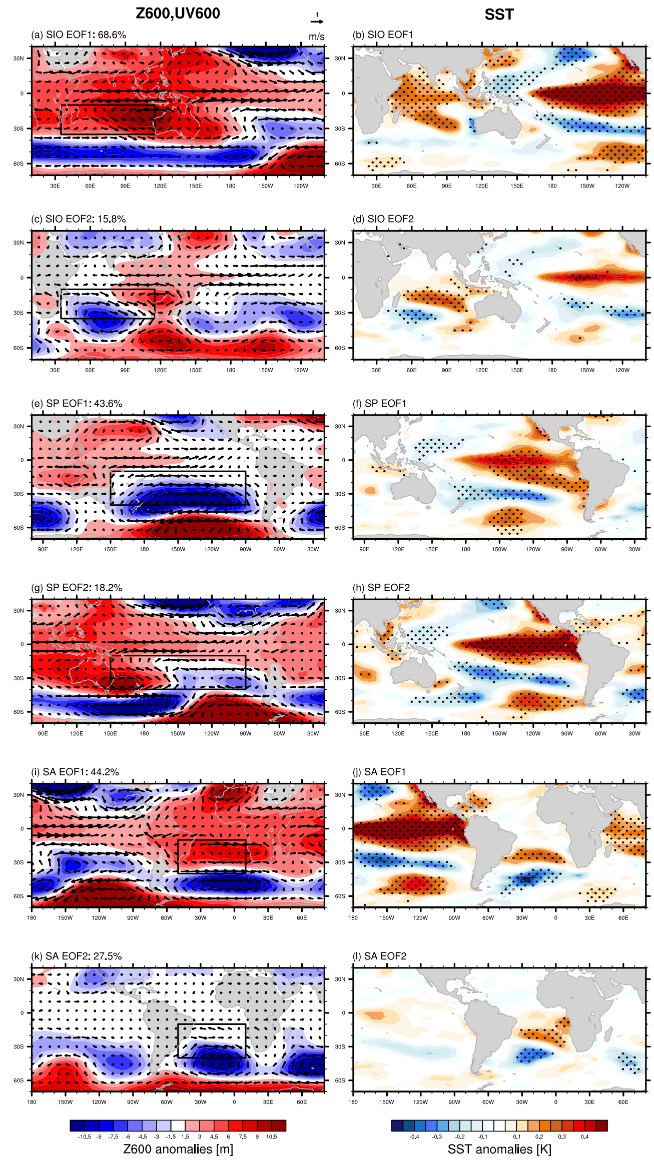

FIG. 6. The first and second modes of the Z600 anomaly field (box region) in the (a,c) South Indian Ocean, (e,g) South Pacific, and (i,k) South Atlantic during December–January via EOF analysis. Respective PC1 and PC2s are regressed on the Z600 and UV600 anomaly fields for the (a,c) South Indian Ocean, (e,g) South Pacific, and (i,k) South Atlantic. Similarly, PC1 and PC2 regressed on SST in the (b,d) South Indian Ocean, (f,h) South Pacific, and (j,l) South Atlantic. The dotted region indicates statistical significance above the 95% level using Student's t-test for SST anomalies.

broad region of anomalous descending motion over the tropical Southern Indian Ocean overlying negative SST anomalies associated with the positive SIOD (Figs. 7e-f). Accompanying this broad

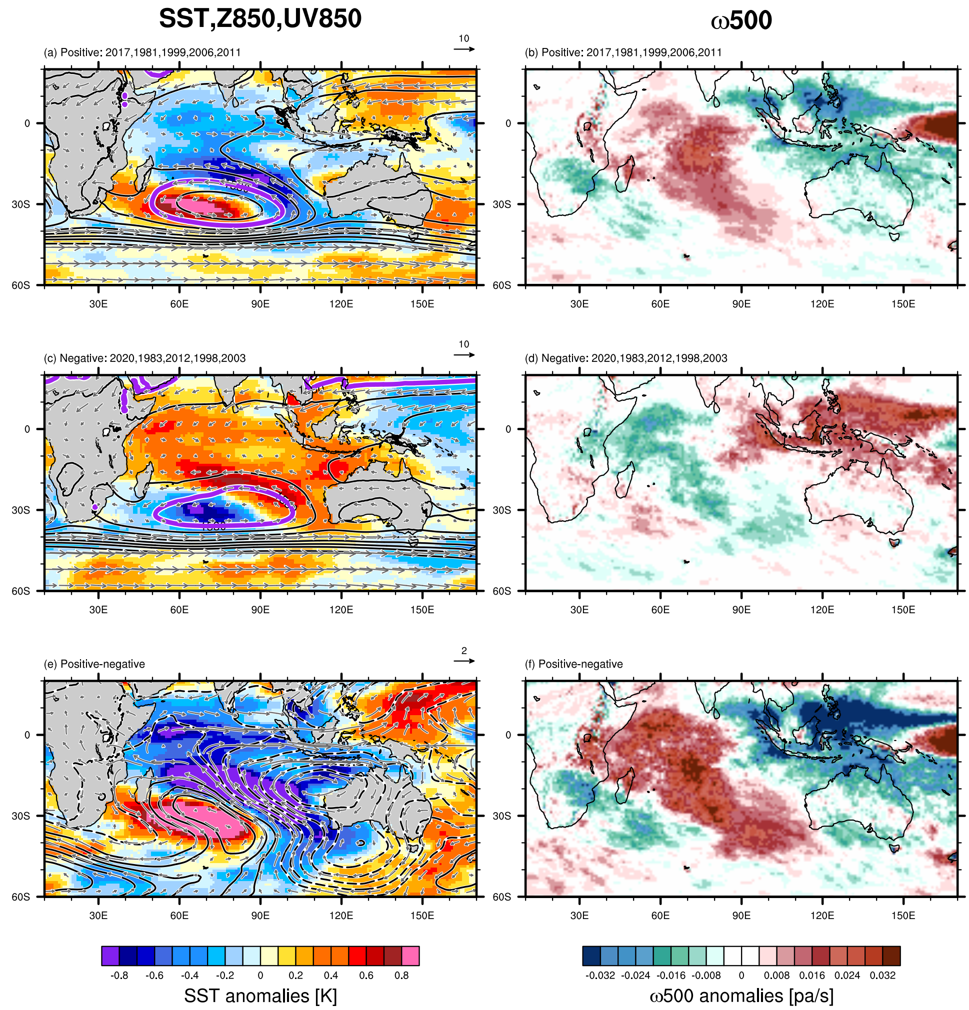

FIG. 7. (a,c) South Indian Ocean SST dipole composite seasons using SST anomalies (colors), Z850 (contours), UV850 (arrows), and (b,d) OLR anomalies (colors). Contours are every 15 geopotential meters. The 1530 m contour is purple to depict the South Indian Ocean STH. Arrows are in m/s and defined at the top right of each plot. (d,e) The relative difference between positive and composite seasons where (e) contours are every 4 geopotential meters.

region of anomalous descending motion is anomalous equatorward flow, which is consistent with Sverdrup effects (Seager et al. 2003).

d. Landfall probability modulated by changes in western peripheries of STH cells

We identified three basins with abundant TC activity and significant variability on the western edge of the basin's STH that respond to anomalous SST gradients: The North Pacific, North

Atlantic, and South Indian Ocean. We now examine whether a relationship exists between these anomalous SST dipoles and TC landfall probability in the northern hemisphere in Figure 8 using the same composite seasons as in Figure 4. We apply the same framework in the South Indian Ocean in Figure 9 using composite seasons as in Figure 7.

In the Western North Pacific basin, Figure 8a and 8c show TC tracks for positive and negative composite cases (same seasons as Fig. 4). The mean track for the positive composites (thick black track) in Figure 8a depicts a stark difference compared to the negative case, with the mean longitude of curving occurring $\sim 6°$ farther west near the East Asia coastline in the positive case. In other words, the positive SST inter-basin dipole: cold in the western North Pacific and warm in the South China Sea and north Indian Ocean, accompanies a shift in TC tracks due to changes in the steering flow at 850 hPa as shown in Figure 4. Interestingly, there were fewer TCs in the WNP basin for positive composite seasons compared to the negative composite due to the negative SST anomalies that accompany inhibiting thermodynamic environmental conditions. Meanwhile, the negative composite depicts positive SST anomalies in the WNP basin that promotes TC genesis (43 vs. 71 total TCs). Due to reduced TC activity during the positive composite, fewer TCs make landfall in the positive composite, but the probability of landfall is higher in the positive composite compared to the negative composites (77% vs. 73%). In other words, when we have a positive inter-basin SST dipole, the westward extension promotes increased seasonal landfall risk if TCs form. This percentage difference is not statistically significant, possibly due to the spatial variations in TC genesis and subsequent landfall probability (Johnson et al. 2022).

In the North Atlantic, Figure 8b and 8d paint an alternative story. During a positive inter-basin SST dipole, comprised of anomalously cold SST anomalies over the main development region and anomalously warm SSTs over the midlatitude North Atlantic ($30-40°$N), TC genesis is suppressed. Figure 8b shows almost no TCs in the Caribbean and the Gulf of Mexico, and few over the main development region. Notably, a negative relationship exists between seasonal SST anomalies associated with the inter-basin SST dipole and seasonal TC genesis frequency in the North Atlantic Basin ($R = -0.33$). Meanwhile, during a negative inter-basin SST dipole, comprised of anomalously warm SSTs in the main development region and the Caribbean, Figure 8d shows abundant TC activity over these regions. As a result, Figure 8b depicts composite mean genesis ~ 414 km farther to the south during negative inter-basin dipole compared to the positive

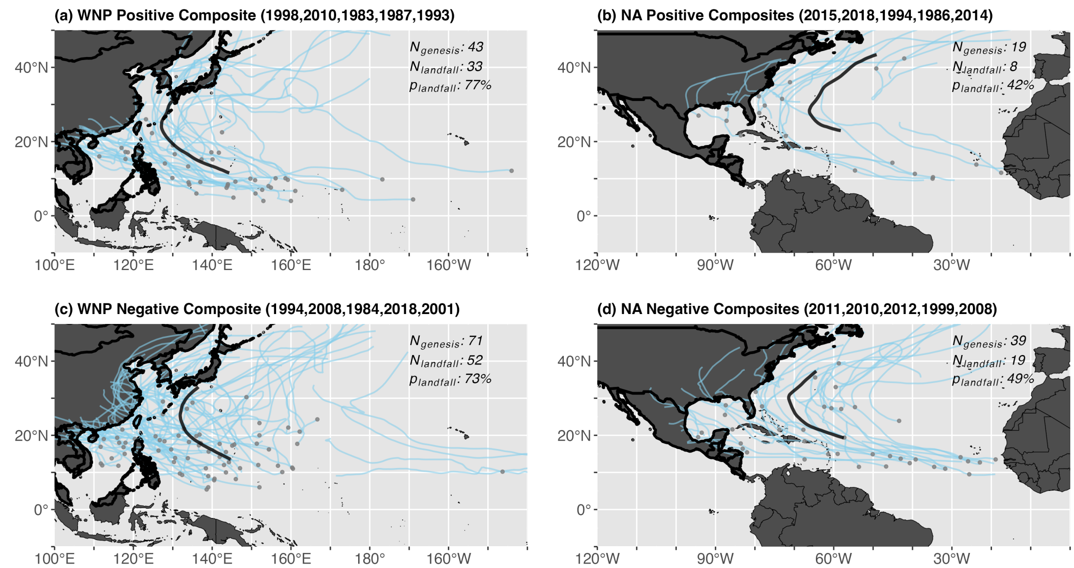

FIG. 8. (a,b) Positive composites and (c,d) negative composites of the inter-basin SST dipoles in the Indo-Pacific region (a,c) and eastern North Pacific-North Atlantic region (b,d), using composite seasons as in Figure 4a-c

.

composites, suggesting more TCs are embedded in easterly flow on the southern periphery of the STH rather than the midlatitude flow farther north. Figures 4d and 8d clearly show mean genesis favors regions of anomalously warm SSTs in the northern tropical Atlantic during the negative composites. Many TCs form in the anomalously warm Caribbean or Gulf of Mexico (Hart et al. 2016). As a result of the southward shift of mean TC genesis during a negative inter-basin SST dipole, more TCs are embedded in the equatorward side of STHs, favoring a higher likelihood of making landfall over Central and North America. Whereas mean TC genesis is farther north in the open Atlantic for the positive case, TCs are more likely to recurve out into the open North Atlantic, where they weaken and dissipate. In other words, only 7 of 19 TCs form south of 20°N in the positive composites (Fig. 8b), whereas 23 of 29 form south 20°N in negative composites (Fig. 8d). Alternatively, the anomalously warm SSTs in the north Tropical Pacific may be related to ENSO-like warming (Fig. 4b), which would further inhibit Atlantic TC development through the enhancement of vertical wind shear and reduced relative humidity (Gray 1984; Shapiro 1987; Goldenberg and Shapiro 1996; Camargo et al. 2007). In the North Atlantic, anomalously warm

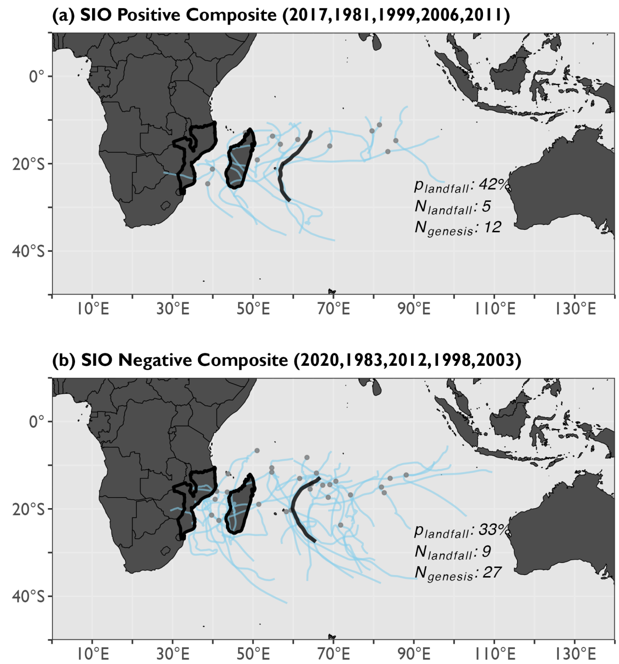

FIG. 9. (a) Positive composites and (b) negative composites of the SST dipole in the Southern Indian Ocean using composite seasons as in Figure 7a-c. Note that only TCs west of 90°E are analyzed in the Southern Indian Ocean basin.

.

SSTs may be related to the Atlantic Meridional Mode (AMM) or Atlantic Multidecadal Variability (AMV) (Enfield et al. 2001; Kossin and Vimont 2007; Zhang et al. 2019).

In the Southern Indian Ocean, Figure 9 depicts the mean track ~ 4° shifted to the west in the positive composites compared to the negative composites. This result complements a northwestward expansion of the Southern Indian Ocean STH during the positive SIO dipole phase, leading to a more favorable steering flow pattern for increased seasonal landfall probability (Fig. 7). Notably, more TCs form in the negative composite due to anomalously warm SSTs in the main development region of the Southern Indian Ocean. Yet, the probability of landfall is less because the steering flow pattern is weaker (Fig. 7e). Whereas, in the positive composite, the composite mean steering flow favors TCs to be directed into Madagascar and Mozambique owing to the stronger pressure gradient (Fig. 7). As a result, a positive SIOD favors an increase in seasonal landfall probability (42% vs. 33%). The above composites are not significantly different from one another based on a two-proportions z-test (P-value of 0.85, 0.85, and 0.89 for the WNP, NA, and SIO), yet trajectory changes in Figures 8 and 9 and past research support an STH impact on TC landfall probability (e.g., Wang et al. 2013; Li et al. 2020; Johnson et al. 2022).

e. Synthesizing global STH behavior

Intrahemispheric STHs in the northern hemisphere behave harmonically in their seasonal evolution, and their westward extensions respond to similar SST patterns (Fig. 1). Seasonally, the North Atlantic and North Pacific synchronously strengthen in boreal spring, depicting similar structure and seasonal evolution. By summer in both hemispheres, significant variability on the western periphery of both STHs emerges, where we find Earth's warmest waters and abundant TC activity. The summertime westward extensions of both STHs have dependencies with anomalous inter-basin SST patterns: warm west and cold east, that induce anomalous lower-tropospheric easterlies in 10–20°N band (Fig. 10). Interestingly, the topographical features underlying the cross-basin easterly winds have key differences. Indonesia, Philippines, and Malaysia, separating the inter-basin SST gradient relevant for the North Pacific STH, comprise of gappy islands. Whereas Central America is mountainous (elevation > 2000 m). These topographical features may explain the weaker anomalous easterlies relevant for the westward extension of the North Atlantic STH (Fig. 8b vs. 8d). In contrast to NH STHs, SH STHs appear year-round and have less seasonality. Yet, intrahemispheric STHs in the SH have key differences. While the South Pacific STH is exceedingly stable year-round, the South Indian Ocean and South Atlantic STHs are characterized by a seasonal zonal movement from west to east and back to the west in austral spring, summer, and fall, respectively (Fig. 1).

The seasonal stability in SH STHs is akin to aquaplanet simulations of STHs where the midlatitude westerly jet is robust and zonally symmetric, highlighting the key interhemispheric difference between NH and SH STHs (Merlis and Held 2019; Yang et al. 2022). Southern hemispheric STHs are pronounced at any given season, while northern hemispheric STHs are only pronounced during the summertime owing to the wintertime wavy midlatitude jet and summertime monsoonal heating (Fig. 1) (Seager et al. 2003). Through the inter-basin perspective, within the 10–20°S band, large landmasses separate the South Pacific, South Atlantic, and South Indian Oceans, highlighting a stark difference compared to the northern hemisphere. As a result, the large landmasses will inhibit inter-basin zonal pressure gradients that respond to inter-basin SST gradients, suppressing

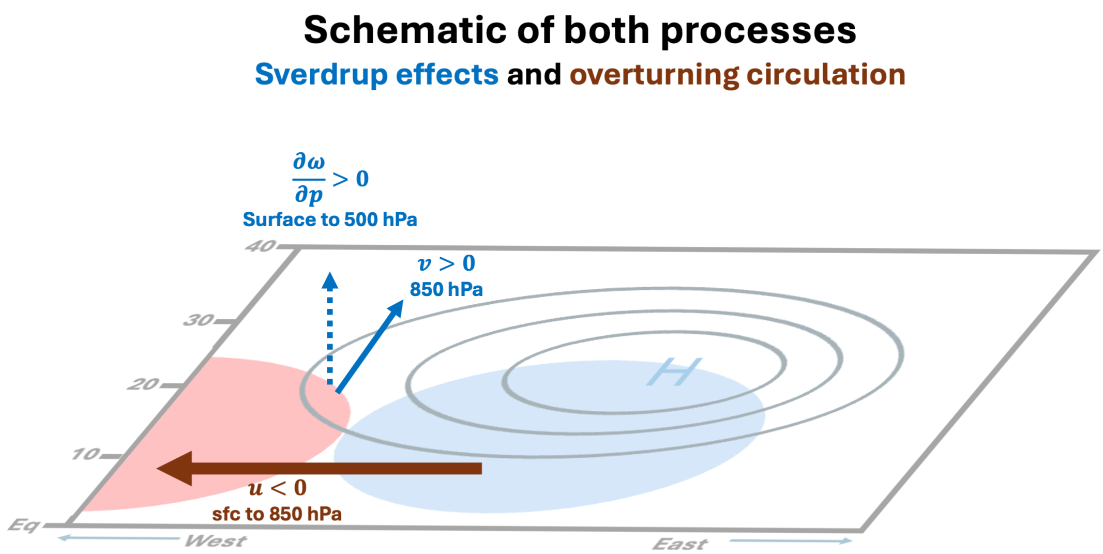

FIG. 10. Schematic of both physical processes to describe the westward extension of the STH based on an inter-basin SST gradient in the northern hemisphere. Opaque background depicts a westward extension of a STH at 850 hPa coinciding with an inter-basin SST gradient: warm west and cool east. Blue arrows depict the Sverdrup effects that promote poleward flow, whereas brown arrow in the tropics supports the overturning circulation at 850 hPa.

any westward extensions of STHs. This perspective supports that the zonal variability in the Southern Indian Ocean STH responds to localized SST gradients, not inter-basin SSTs. Anomalous zonal SST gradients in the northern hemisphere relevant for the western peripheries of STHs have land-atmosphere effects, obscuring Sverdrup effects in observations, whereas the anomalous zonal gradient in the Southern Indian Ocean is over open water, far from land, which promotes Sverdrup effects.

4. Discussion and conclusion

Changes in STHs, linked to ocean-atmosphere interactions, lead to changes in steering flow for TCs. This work examined dependencies of zonal SST gradients on changes on the western peripheries of STHs and, subsequently, linked them to early seasonal changes in TC landfall probability in June–August in the northern hemisphere and December–February in the southern hemisphere. In the northern hemisphere, anomalous zonal inter-basin SST gradients support westward extensions of the North Pacific and North Atlantic STHs, whereas the South Indian Ocean SST dipole supports a northwest expansion of the South Indian Ocean STH. The key findings of this study are as follows:

1. Summertime STHs exhibit significant variability on their western edges.
2. An inter-basin zonal SST gradient between the western North Pacific and North Indian Ocean promotes a westward extension of the Pacific STH. Similarly, an inter-basin SST gradient between the North Tropical Atlantic and eastern North Pacific promotes a westward extension of the North Atlantic STH.
3. A localized South Indian Ocean SST dipole promotes a northwest expansion of the South Indian Ocean STH.
4. The Indo-Pacific inter-basin SST gradient is associated with a 4% increase in early-seasonal WNP TC landfall probability, while the Pacific-Atlantic inter-basin SST gradient is associated with a 7% decrease in early seasonal NA TC landfall probability.
5. The South Indian Ocean SST dipole is associated with a 12% increase in early seasonal TC landfall probability.
6. In contrast with northern hemispheric STHs responding to inter-basin SST gradients, topographical effects regionally constrain STH variability to their respective basin in the southern hemisphere.
7. Variability on the western edge of the South Indian Ocean is in agreement with the Sverdrup effects owing to atmospheric vertical motions that respond to anomalous zonal SST gradients.
8. Sverdrup effects may play a secondary role in the western edges of northern hemispheric STHs.

In the northern hemisphere, anomalous inter-basin SST gradients north of the equator trigger cross-continental easterly wind anomalies in the lower troposphere, promoting a westward extension of the North Pacific and North Atlantic STHs. The North Pacific STH extends $\sim 15^\circ$ in longitude farther west during a positive inter-basin SST dipole, which is comprised of positive SST anomalies extending from the North Indian Ocean to the South China Sea and negative SST anomalies that extend southwest from the Hawaiian Islands. The North Atlantic STH extends $\sim 12°$ in longitude farther west during a positive inter-basin SST dipole, which is comprised of positive SST anomalies in the northeast tropical Pacific (adjacent to Mexico mainland) and negative SST anomalies over the North Tropical Atlantic region. Alternatively, the westward extension of the North Pacific STH may be related to an El Niño decaying pattern (Du et al. 2011; Zhan et al. 2011; Chung and Li 2015), and the westward extension of the North Atlantic STH may respond to tropical upper-tropospheric troughs (Wang et al. 2020) or the North Atlantic Oscillation (Portis et al. 2001; Folland et al. 2009; Murakami et al. 2016), or simply localized SST variations (Wu et al. 2010).

Our results in the Southern Indian Ocean align with the mechanisms proposed by Rodwell and Hoskins (2001) and Seager et al. (2003), while offering a distinct perspective for northern hemispheric STHs. They recognized STHs primarily satisfy the Sverdrup balance framework (Sverdrup et al. 1942), where basin zonal SST gradients: positive west and negative east, contribute to poleward motion on the western edge and equatorward motion on the eastern edge of basins. Here, we focus on the western edge of the North Atlantic and North Pacific STHs and find that north tropical anomalous inter-basin SST gradients lead to anomalous easterlies and increased heights on the western peripheries of STHs. Our result is reminiscent of zonal overturning circulation (i.e., Walker circulation). To complete the anomalous circulation, anomalous poleward flow occurs underneath ascending motions, and anomalous equatorward flow occurs underneath descending motions, in accordance with anomalous Sverdrup effects.

Southern hemispheric STH variability tends to be primarily linked to ENSO. The South Pacific STH seems to have minimal dependencies on anomalous zonal SST gradients. In the South Indian Ocean, an El Niño is linked to a strengthened South Indian Ocean STH. However, the second mode of the South Indian Ocean STH shows a zonal contrast in STH variability. Further analysis links zonal STH variability to the South Indian Ocean SST dipole, where its positive phase leads to a northwest expansion of the South Indian Ocean STH (Behera et al. 2000; Behera and Yamagata 2001; Reason 2001; England et al. 2006). As a result, increased easterlies where there is abundant TC activity lead to a $\sim 9\%$ increase in TC landfall probability impacting Madagascar and Mozambique. These results suggest that TC forecasters in the Southern Indian Ocean need to carefully assess the phase of the South Indian Ocean SST dipole to help mitigate seasonal TC landfall risk.

Based on past research and the results presented here, STHs are complex to understand, with many mechanisms to describe their structure, strength, and location. Here, we take an ocean-atmospheric perspective; however, STHs are also initially forced by land-atmospheric and land-sea effects (Hoskins 1996). Our analysis shows that the western edges of STHs are highly variable, independent of the central STH strength, and appear to be linked to anomalous inter-basin SST gradients in the northern hemisphere, with ENSO having a greater effect on STHs in the southern hemisphere. Alternatively, remote SST precursors in the tropical Atlantic may also contribute to variability on the western periphery of the North Pacific STH through inter-basin interactions (Zuo et al. 2019; Cai et al. 2019; Chikamoto et al. 2020). The analysis here is simply based on historical data. Climate model experiments that constrain ocean variability are required to provide a more robust assessment to link SST gradients and STH variability, especially on the western edge where we typically see active ocean-atmosphere coupling.

Acknowledgments. ZFJ, JJJ, and DRC were supported through NSF grant number 1945113. YC is supported by the Utah Agricultural Experiment Station, Utah State University (approved as journal paper #9833), U.S. Geological Survey and Utah Center for Water Resources Research for the 104b grant (G21AP10623-04), the U.S. Department of Interior, Bureau of Reclamation (R22AP00220 and R24AP00321), the Strategic Environmental Research and Development Program (RC20-3056), and a US Department of Energy grant (DESC0016605). HR acknowledges funding from the Climate Systems Hub of the Australian Government's National Environmental Science Program (NESP). The authors thank Chris Landsea and two anonymous reviewers for their invaluable feedback that improved this paper.

Data availability statement. All data used in this study can be obtained free of charge to any member of the public. COBE-SST and NCEP data can be obtained from NOAA/OAR/ESRL PSD, Boulder, Colorado, USA. ERA5 can be obtained from ECMWF Copernicus. All analyses and plotting were performed using the NCAR command language (NCL), Python, and R. The code in this study can be requested from the corresponding author.

References

Behera, S., P. Salvekar, and T. Yamagata, 2000: Simulation of interannual sst variability in the tropical indian ocean. *Journal of Climate*, **13 (19)**, 3487–3499.

Behera, S. K., and T. Yamagata, 2001: Subtropical sst dipole events in the southern indian ocean. *Geophysical Research Letters*, **28 (2)**, 327–330.

Broccoli, A. J., and S. Manabe, 1992: The effects of orography on midlatitude northern hemisphere dry climates. *Journal of Climate*, **5 (11)**, 1181–1201.

Cai, W., and Coauthors, 2019: Pantropical climate interactions. *Science*, **363 (6430)**, eaav4236.

Camargo, S. J., K. A. Emanuel, and A. H. Sobel, 2007: Use of a genesis potential index to diagnose enso effects on tropical cyclone genesis. *Journal of Climate*, **20 (19)**, 4819–4834.

Camp, J., and Coauthors, 2019: The western pacific subtropical high and tropical cyclone landfall: Seasonal forecasts using the met office glosea5 system. *Quarterly Journal of the Royal Meteorological Society*, **145 (718)**, 105–116.

Chikamoto, Y., Z. Johnson, S.-Y. S. Wang, M. McPhaden, and T. Mochizuki, 2020: El niño–southern oscillation evolution modulated by atlantic forcing. *Journal of Geophysical Research: Oceans*, **125 (8)**, e2020JC016 318.

Chikamoto, Y., and Coauthors, 2015: Skilful multi-year predictions of tropical trans-basin climate variability. *Nature communications*, **6 (1)**, 6869.

Choi, J., J. Lu, S.-W. Son, D. M. Frierson, and J.-H. Yoon, 2016: Uncertainty in future projections of the north pacific subtropical high and its implication for california winter precipitation change. *Journal of Geophysical Research: Atmospheres*, **121 (2)**, 795–806.

Chung, P.-h., and T. Li, 2015: Characteristics of tropical cyclone genesis in the western north pacific during the developing and decaying phases of two types of el niño. *Journal of Tropical Meteorology*, **21 (1)**, 14.

DeMaria, M., and Coauthors, 2022: The national hurricane center tropical cyclone model guidance suite. *Weather and Forecasting*, **37 (11)**, 2141–2159.

Du, Y., L. Yang, and S.-P. Xie, 2011: Tropical indian ocean influence on northwest pacific tropical cyclones in summer following strong el niño. *Journal of Climate*, **24 (1)**, 315–322.

Enfield, D. B., A. M. Mestas-Nuñez, and P. J. Trimble, 2001: The atlantic multidecadal oscillation and its relation to rainfall and river flows in the continental us. *Geophysical research letters*, **28 (10)**, 2077–2080.

England, M. H., C. C. Ummenhofer, and A. Santoso, 2006: Interannual rainfall extremes over southwest western australia linked to indian ocean climate variability. *Journal of Climate*, **19 (10)**, 1948–1969.

Folland, C. K., J. Knight, H. W. Linderholm, D. Fereday, S. Ineson, and J. W. Hurrell, 2009: The summer north atlantic oscillation: past, present, and future. *Journal of Climate*, **22 (5)**, 1082–1103.

Gamble, D. W., D. B. Parnell, and S. Curtis, 2008: Spatial variability of the caribbean mid-summer drought and relation to north atlantic high circulation. *International Journal of Climatology: A Journal of the Royal Meteorological Society*, **28 (3)**, 343–350.

Gill, A. E., 1980: Some simple solutions for heat-induced tropical circulation. *Quarterly Journal of the Royal Meteorological Society*, **106 (449)**, 447–462.

Gilliland, J. M., and B. D. Keim, 2018: Position of the south atlantic anticyclone and its impact on surface conditions across brazil. *Journal of Applied Meteorology and Climatology*, **57 (3)**, 535–553.

Goldenberg, S. B., and L. J. Shapiro, 1996: Physical mechanisms for the association of el niño and west african rainfall with atlantic major hurricane activity. *Journal of Climate*, **9 (6)**, 1169–1187.

Gray, W. M., 1984: Atlantic seasonal hurricane frequency. part i: El niño and 30 mb quasi-biennial oscillation influences. *Monthly weather review*, **112 (9)**, 1649–1668.

Ham, Y.-G., J.-S. Kug, J.-Y. Park, and F.-F. Jin, 2013: Sea surface temperature in the north tropical atlantic as a trigger for el niño/southern oscillation events. *Nature Geoscience*, **6 (2)**, 112–116.

Hart, R. E., D. R. Chavas, and M. P. Guishard, 2016: The arbitrary definition of the current atlantic major hurricane landfall drought. *Bulletin of the American Meteorological Society*, **97 (5)**, 713–722.

He, C., and T. Zhou, 2015: Responses of the western North Pacific subtropical high to global warming under RCP4. 5 and RCP8. 5 scenarios projected by 33 CMIP5 models: The dominance of tropical Indian Ocean–tropical western Pacific SST gradient. *Journal of Climate*, **28 (1)**, 365–380.

Hersbach, H., 2016: The era5 atmospheric reanalysis. *AGU fall meeting abstracts*, Vol. 2016, NG33D–01.

Ho, C.-H., J.-H. Kim, J.-H. Jeong, H.-S. Kim, and D. Chen, 2006: Variation of tropical cyclone activity in the south indian ocean: El niño–southern oscillation and madden-julian oscillation effects. *Journal of Geophysical Research: Atmospheres*, **111 (D22)**.

Hoskins, B., 1996: On the existence and strength of the summer subtropical anticyclones: Bernhard haurwitz memorial lecture. *Bulletin of the American Meteorological Society*, **77 (6)**, 1287–1292.

Huang, Y., H. Wang, K. Fan, and Y. Gao, 2015: The western pacific subtropical high after the 1970s: westward or eastward shift? *Climate Dynamics*, **44 (7)**, 2035–2047.

Ishii, M., A. Shouji, S. Sugimoto, and T. Matsumoto, 2005: Objective analyses of sea-surface temperature and marine meteorological variables for the 20th century using icoads and the kobe collection. *International Journal of Climatology: A Journal of the Royal Meteorological Society*, **25 (7)**, 865–879.

Johnson, Z. F., D. R. Chavas, and H. A. Ramsay, 2022: Statistical framework for western north pacific tropical cyclone landfall risk through modulation of the western pacific subtropical high and enso. *Journal of Climate*, 1–32.

Jones, J. J., D. R. Chavas, and Z. F. Johnson, 2024: Inter-basin versus intra-basin sea surface temperature forcing of the western north pacific subtropical high's westward extensions. *Journal of Geophysical Research: Atmospheres*, **129 (15)**, e2023JD040 429.

Knaff, J. A., 1997: Implications of summertime sea level pressure anomalies in the tropical atlantic region. *Journal of climate*, **10 (4)**, 789–804.

Knapp, K. R., M. C. Kruk, D. H. Levinson, H. J. Diamond, and C. J. Neumann, 2010: The international best track archive for climate stewardship (ibtracs) unifying tropical cyclone data. *Bulletin of the American Meteorological Society*, **91 (3)**, 363–376.

Kosaka, Y., S.-P. Xie, N.-C. Lau, and G. A. Vecchi, 2013: Origin of seasonal predictability for summer climate over the Northwestern Pacific. *Proceedings of the National Academy of Sciences*, **110 (19)**, 7574–7579.

Kossin, J. P., and D. J. Vimont, 2007: A more general framework for understanding atlantic hurricane variability and trends. *Bulletin of the American Meteorological Society*, **88 (11)**, 1767–1782.

Li, B., L. Zhou, T. Lian, T. Liu, J. Qin, Y. Du, and D. Chen, 2023: Impacts of sea surface temperature gradient on monsoon intraseasonal oscillation. *Journal of Climate*, **36 (4)**, 1161–1173.

Li, H., F. Xu, and Y. Lin, 2020: The impact of sst on the zonal variability of the western pacific subtropical high in boreal summer. *Journal of Geophysical Research: Atmospheres*, **125 (11)**, e2019JD031 720.

Liess, S., and M. A. Geller, 2012: On the relationship between qbo and distribution of tropical deep convection. *Journal of Geophysical Research: Atmospheres*, **117 (D3)**.

Lu, R., and B. Dong, 2001: Westward extension of North Pacific subtropical high in summer. *Journal of the Meteorological Society of Japan. Ser. II*, **79 (6)**, 1229–1241.

Maloney, E. D., and S. K. Esbensen, 2003: The amplification of east pacific madden–julian oscillation convection and wind anomalies during june–november. *Journal of climate*, **16 (21)**, 3482–3497.

Matsuno, T., 1966: Quasi-geostrophic motions in the equatorial area. *Journal of the Meteorological Society of Japan. Ser. II*, **44 (1)**, 25–43.

Merlis, T. M., and I. M. Held, 2019: Aquaplanet simulations of tropical cyclones. *Current Climate Change Reports*, **5**, 185–195.

Miyasaka, T., and H. Nakamura, 2010: Structure and mechanisms of the southern hemisphere summertime subtropical anticyclones. *Journal of climate*, **23 (8)**, 2115–2130.

Murakami, H., G. Villarini, G. A. Vecchi, W. Zhang, and R. Gudgel, 2016: Statistical–dynamical seasonal forecast of north atlantic and us landfalling tropical cyclones using the high-resolution gfdl flor coupled model. *Monthly Weather Review*, **144 (6)**, 2101–2123.

Portis, D. H., J. E. Walsh, M. El Hamly, and P. J. Lamb, 2001: Seasonality of the north atlantic oscillation. *Journal of Climate*, **14 (9)**, 2069–2078.

Reason, C., 2001: Subtropical indian ocean sst dipole events and southern african rainfall. *Geophysical Research Letters*, **28 (11)**, 2225–2227.

Rodwell, M. J., and B. J. Hoskins, 2001: Subtropical anticyclones and summer monsoons. *Journal of Climate*, **14 (15)**, 3192–3211.

Seager, R., R. Murtugudde, N. Naik, A. Clement, N. Gordon, and J. Miller, 2003: Air–sea interaction and the seasonal cycle of the subtropical anticyclones. *Journal of climate*, **16 (12)**, 1948–1966.

Shapiro, L. J., 1987: Month-to-month variability of the atlantic tropical circulation and its relationship to tropical storm formation. *Monthly Weather Review*, **115 (11)**, 2598–2614.

Shaw, T. A., O. Miyawaki, and A. Donohoe, 2022: Stormier southern hemisphere induced by topography and ocean circulation. *Proceedings of the National Academy of Sciences*, **119 (50)**, e2123512 119.

Shuqing, S., and Y. Ming, 1999: Subtropical high anomalies over the western pacific and its relations to the asian monsoon and sst anomaly. *Advances in Atmospheric Sciences*, **16 (4)**, 559–568.

Stuecker, M. F., 2018: Revisiting the pacific meridional mode. *Scientific reports*, **8 (1)**, 1–9.

Sverdrup, H. U., M. W. Johnson, R. H. Fleming, and Coauthors, 1942: *The Oceans: Their physics, chemistry, and general biology*, Vol. 1087. Prentice-Hall New York.

Wang, B., B. Xiang, and J.-Y. Lee, 2013: Subtropical high predictability establishes a promising way for monsoon and tropical storm predictions. *Proceedings of the National Academy of Sciences*, **110 (8)**, 2718–2722.

Wang, C., and S.-K. Lee, 2009: Co-variability of tropical cyclones in the north atlantic and the eastern north pacific. *Geophysical Research Letters*, **36 (24)**.

Wang, H., and M. Ting, 1999: Seasonal cycle of the climatological stationary waves in the ncep–ncar reanalysis. *Journal of the atmospheric sciences*, **56 (22)**, 3892–3919.

Wang, Z., G. Zhang, T. J. Dunkerton, and F.-F. Jin, 2020: Summertime stationary waves integrate tropical and extratropical impacts on tropical cyclone activity. *Proceedings of the National Academy of Sciences*, **117 (37)**, 22 720–22 726.

Wright, K. T., and Coauthors, 2022: Precipitation in northeast mexico primarily controlled by the relative warming of atlantic ssts. *Geophysical Research Letters*, **49 (11)**, e2022GL098 186.

Wu, B., T. Li, and T. Zhou, 2010: Relative Contributions of the Indian Ocean and Local SST Anomalies to the Maintenance of the Western North Pacific Anomalous Anticyclone during the El Niño Decaying Summer. *Journal of Climate*, **23 (11)**, 2974 – 2986.

Wu, L., B. Wang, and S. Geng, 2005: Growing typhoon influence on east asia. *Geophysical Research Letters*, **32 (18)**.

Yang, H., J. Lu, Q. Wang, X. Shi, and G. Lohmann, 2022: Decoding the dynamics of poleward shifting climate zones using aqua-planet model simulations. *Climate Dynamics*, **58 (11-12)**, 3513–3526.

Yun, K.-S., K.-J. Ha, S.-W. Yeh, B. Wang, and B. Xiang, 2015: Critical role of boreal summer north pacific subtropical highs in enso transition. *Climate Dynamics*, **44 (7)**, 1979–1992.

Zhan, R., Y. Wang, and C.-C. Wu, 2011: Impact of ssta in the east indian ocean on the frequency of northwest pacific tropical cyclones: A regional atmospheric model study. *Journal of Climate*, **24 (23)**, 6227–6242.

Zhang, R., R. Sutton, G. Danabasoglu, Y.-O. Kwon, R. Marsh, S. G. Yeager, D. E. Amrhein, and C. M. Little, 2019: A review of the role of the atlantic meridional overturning circulation in atlantic multidecadal variability and associated climate impacts. *Reviews of Geophysics*, **57 (2)**, 316–375.

Zhou, T., and Coauthors, 2009: Why the western pacific subtropical high has extended westward since the late 1970s. *Journal of Climate*, **22 (8)**, 2199–2215.

Zuo, J., W. Li, C. Sun, and H.-C. Ren, 2019: Remote forcing of the northern tropical atlantic sst anomalies on the western north pacific anomalous anticyclone. *Climate Dynamics*, **52**, 2837–2853.